Subscriber access provided by NATL INST STANDARDS & TECH

Article

Relaxation Behavior of Polymer Structures Fabricated by Nanoimprint Lithography

Yifu Ding, Hyun Wook Ro, Thomas A. Germer, Jack F. Douglas, Brian C. Okerberg, Alamgir Karim, and Christopher L. Soles

ACS Nano, **2007**, 1 (2), 84-92 • DOI: 10.1021/nn700014p • Publication Date (Web): 14 August 2007

Downloaded from http://pubs.acs.org on December 11, 2008

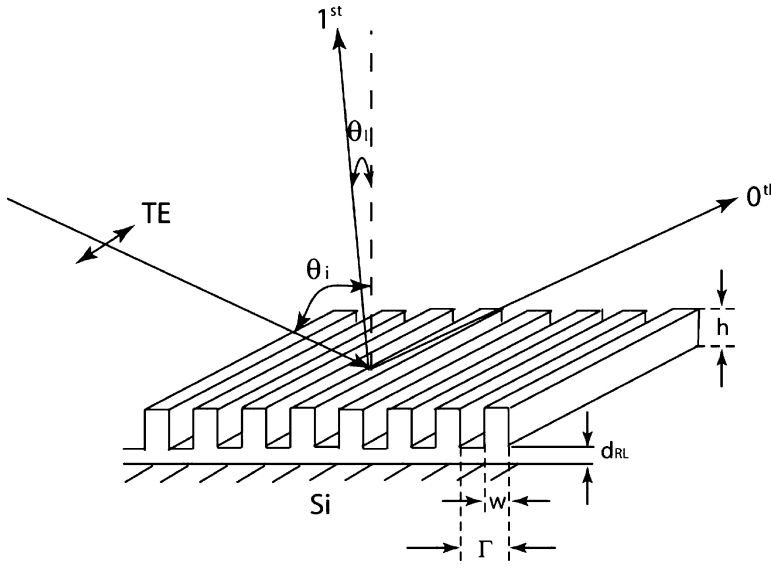

More About This Article

Additional resources and features associated with this article are available within the HTML version:

- Supporting Information
- Links to the 4 articles that cite this article, as of the time of this article download
- Access to high resolution figures
- Links to articles and content related to this article
- Copyright permission to reproduce figures and/or text from this article

View the Full Text HTML

ACS Publications
High quality. High impact.

ACS Nano is published by the American Chemical Society. 1155 Sixteenth Street N.W., Washington, DC 20036

ARTICLE

Relaxation Behavior of Polymer Structures Fabricated by Nanoimprint Lithography

Yifu Ding,[†] Hyun Wook Ro,[†] Thomas A. Germer,[‡] Jack F. Douglas,[†] Brian C. Okerberg,[†,§] Alamgir Karim,[†] and Christopher L. Soles[†,*]

[†]Polymers Division, National Institute of Standards and Technology, 100 Bureau Drive, Gaithersburg, Maryland 20899-8541, and [‡]Optical Technology Division, National Institute of Standards and Technology, 100 Bureau Drive, Gaithersburg, Maryland 20899-8443. [§]National Research Council postdoctoral associate.

ABSTRACT We study the decay of imprinted polystyrene (PS) patterns under thermal annealing using light diffraction. The first-order diffraction intensity from the imprinted gratings was measured as a function of annealing time. A local intensity maximum is observed as a function of annealing time. This "abnormal" intensity variation can be qualitatively understood, using rigorous coupled wave approximation calculations, as a characteristic diffraction from patterns with specific shape/height. We demonstrate that this diffraction anomaly can be used to characterize the temperature dependence of the pattern decay rate. The activation energies of the pattern decay are found to be similar to those of the segmental and chain relaxations. Comparisons between PS samples of different molecular mass reveal that the patterns decay through different mechanisms. For unentangled PS, the decay of the imprinted pattern follows the surface-tension-driven viscous flow, with a viscosity similar to the steady-state viscosity. However, for highly entangled PS, large residual stresses introduced from the imprinting process cause the pattern to decay much faster than expected from surface-tension-driven viscous flow.

KEYWORDS: nanoimprint lithography · pattern decay · relaxation · stability · thermal embossing

*Address correspondence to csoles@nist.gov.

Received for review April 20, 2007 and accepted July 12, 2007.

Published online August 14, 2007.
10.1021/nn700014p CCC: $37.00

© 2007 American Chemical Society

Nanoimprint lithography (NIL) is quickly maturing as a next-generation patterning technique that offers an alternative to optical lithography.[1–17] NIL is a type of contact lithography where the pattern transfers from a rigid mold to a liquid/melt resist through one of two typical approaches: ultraviolet (UV) radiation-induced cross-linking[1–7] or thermal embossing.[8–17] In the former route, the resist is a liquid film that is "wicked" into the mold *via* capillary effects and cross-linked with UV radiation into a rigid pattern. Thermal embossing NIL utilizes the viscoelastic deformation of a polymeric resist.[8–17] The pattern is transferred to the resist film by mechanically forcing or squeezing the polymer into the mold at elevated temperatures and pressures. When the mold and replica are cooled below the glass transition temperature (T_g) of the polymer, the pressure is released and the mold separated from the replicated polymeric pattern.

An advantage of thermal embossing NIL over other lithographic patterning techniques is its capability of patterning a wide range of polymeric materials. The process is a nanoscale variation of the macroscopic thermal stamping, forming, or injection molding processes used with polymers. Therefore, it has great potential for *directly* patterning functional materials, such as semiconducting polymers,[18,19] dielectric insulators,[20] polymeric photonic crystals,[19,21] block copolymers,[22] piezoelectric polymers,[23] and semicrystalline polymers.[24] Other lithographic techniques usually pattern on a formulated sacrificial resist and transfer the pattern into the functional material by additional additive or subtractive manufacturing processes. The direct patterning of functional materials through thermal embossing NIL has the potential to simplify nanofabrication processes.

Patterns with sub-10 nm features have been successfully fabricated using thermal embossing NIL.[11] At these length scales, the effects of finite size on the physical properties must be considered, and the properties of the polymer can no longer be considered bulk-like.[25–27] For example, deviations in T_g,[25] reductions in the elastic modulus,[26,27] and changes in the thermal expansion coefficient have been reported.[28] Moreover, the constitutive relationship used to guide the macroscopic processing starts to fail when the relevant processing features approach nanoscale dimensions.[29] An understanding of the viscoelastic deformation of a polymer melt squeezing into a nanoscale feature will be required in order to optimize thermal embossing NIL.

Quantifying pattern stability or shape changes due to internal stresses is a chal-lenge in nanoscale patterns. High-resolution, nondestructive measurements are required in order to quantify subtle changes in the shape of an imprinted nanostructure. We are developing a suite of X-ray-based techniques, including critical dimension small-angle X-ray scattering (CD-SAXS) and specular X-ray reflectivity (SXR), to quantify pattern shape with nanometer precision.[30–34] Recently, we have utilized these techniques to illustrate that thermal embossing NIL can introduce large levels of residual stress into the imprinted pattern.[35,36] At elevated temperatures, the NIL-fabricated patterns have a strong propensity to retract in height with very little broadening in the width. A description of these pattern decay measurements is summarized elsewhere.[35,36]

Although both CD-SAXS and SXR with a synchrotron source can provide high-resolution measurements on the pattern evolution, it is impractical to perform real-time measurements over a relatively long time scale. Laboratory-based SXR and CD-SAXS measurements are generally too slow to capture the real-time kinetics. Here, we introduce a simple laser diffraction technique to study the real-time kinetics of the decay of the imprinted polymer grating patterns. The first-order diffraction peak from the imprinted polymer patterns can be obtained using a visible laser, and its intensity is generally related to the amount of material in the grating. By measuring the time and temperature dependence of the diffraction intensity with thermal annealing, one can quantify the pattern decay kinetics. When these kinetic measurements are coupled with complementary high-resolution shape measurements offered by CD-SAXS and SXR, one can develop a detailed understanding of the mechanisms governing the internal stress buildup and stability of the nanoscale patterns fabricated by NIL.

RESULTS AND DISCUSSION

1. Onset Temperature for Pattern Decay. The first experiment was to linearly ramp two different polystyrene (PS) patterns at 2 °C/min from ambient temperatures and record the diffracted intensity as a function of temperature. The intensity of the first-order peak is displayed in Figure 1. For both the PS30k and PS1800k patterns, the intensities do not vary significantly at low temperatures. A large decrease in the diffracted intensity occurs as the temperature increases above 100 °C, indicating that the patterned features are starting to decay toward the flat film. The onset temperature for this pattern decay, T_{onset}, is determined using the intersection of a bilinear fit to be approximately 105 °C for both samples. We note that this value is consistent with the bulk T_g (104 °C) of both materials, as determined by differential scanning calorimetry (DSC). The results suggest that there are no significant variations of the PS T_g values due to the imprint process in this study.

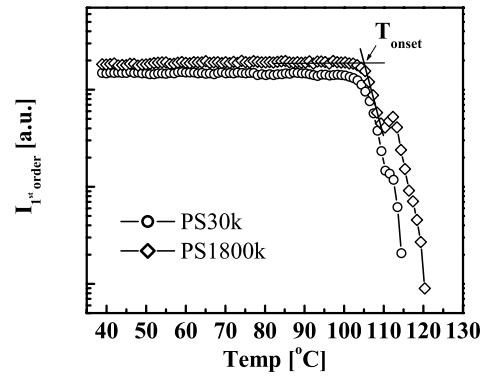

Figure 1. First-order diffraction intensity as a function of temperature. The scan rate is 2 °C/min, and the diffraction intensity was measured at each degree. The circle and diamond symbols represent the PS30k and PS1800k patterns, respectively. The onset temperature of the intensity decay is marked as T_{onset}.

Analogous diffraction methods have been utilized to study the pattern decay of extremely shallow gratings, with amplitudes less than 5 nm, embossed into polymeric surfaces.[37,38] The motivation for these shallow grating experiments was to study the mobility of the polymer surface. Large reductions in the surface T_g were observed for high-molecular-mass poly(methyl methacrylate) (PMMA), while no suppression was observed in low-molecular-mass PMMA.[37] Moreover, recent measurements by Mundra *et al*. showed reduction of T_g for two-dimensional (2D) PMMA nanostructures compared with flat films with similar thickness due to the increase in the ratio of free surface to interfacial area.[39] Reductions in T_g were also reported for both random rough and patterned PS surface with much smaller features (characteristic radius R of the curvature about tens of nanometers), where large Laplace pressures were expected to cause yield at temperatures lower than the bulk T_g,[40,41] inducing the deformation of the surface patterns. It is generally understood that the T_g of planar PS films starts to drop when the thickness decreases below approximately 100 nm.[25] In our case, the size of the PS gratings is much larger (pattern height $h \approx 360$ nm and width $w \approx 240$ nm), and it is possible that our measurements are not sensitive to a change in the surface T_g within a few nanometers of the free surface.

Surprisingly, the diffraction intensity in Figure 1 does not decay monotonically above T_{onset}; a local maximum occurs near 115 °C. This behavior was not observed in analogous diffraction studies of the shallow gratings mentioned above.[37,38] Below, we demonstrate that this abnormal intensity variation is an intrinsic feature resulting from a resonance effect between the light and certain pattern shapes that appear during the annealing. We will also show how this resonance anomaly can be used to investigate the relaxation kinetics of the imprinted patterns.

2. Nature of the Diffraction Local Anomaly. In the application of optical scatterometry, anomalies in the diffraction/reflection intensity as a function of incident wavelength and/or angle are commonly used as distinctive features to calculate the critical dimension of the gratings, such as line width and height.[42] When the periodicity Γ of a grating is much larger than the wavelength of the incident light (λ), the diffraction intensity can be described by the Kirchhoff theory in the Fraunhofer approximation.[43] In this limit, the distribution of diffraction intensity for different orders can be described by a convolution of a Fourier transform of the cross section of a single line (the so-called form factor) and a delta function representing the Bragg condition (the structure factor). A similar analysis is used for diffraction from a series of narrow slits. In the opposite limit, where $\Gamma \ll \lambda$, all the higher orders of diffraction become evanescent, leaving only the zeroth-order diffraction (or specular reflection) peak. In this case, the grating can be treated as an anisotropic film with the refractive index approximated by the effective medium approach (EMA). Between these extremes, when Γ is comparable to λ, the optical response of the grating becomes extremely complicated, and optical resonance effects can arise from the coupling of incident light and guided waves in the structures.[42] The diffraction gratings and the laser used in our experiments fall into this last category.

An exact solution for the diffraction efficiency of such a grating can be calculated using the rigorous coupled wave analysis (RCWA) method.[43,44] The grating is divided into layers for which the index is assumed to vary only in the grating direction. The eigenmodes of each layer are determined with matched boundary conditions for the interfaces between the layers. For light with s-polarization, as in the present case, this method will typically converge on a solution very quickly.

Since the pattern shape evolves upon heating above T_g, we performed calculations for the two extremes: a rectangular line shape representative of the initial grating and a sinusoidal profile characteristic of the profile after long annealing times. At elevated temperatures, the PS patterns should "flow" into the residual layer (causing an increase in d_{RL}; see Materials and Methods), and the patterns evolve into a sinusoidal wave of decreasing amplitude that ultimately progresses toward a flat film. In the RCWA calculations, the volume of the material in the model rectangular and sinusoidal gratings was equal. In the case of the sinusoidal grating, the peak-to-valley amplitude was 360 nm, with a residual layer thickness of 50 nm. We modeled the diffraction intensity as the amplitude of the patterns decayed, and d_{RL} increased to 230 nm [= (360/2 + 50) nm]. For the rectangle, an initial height of 360 nm, a width of 240 nm, and a residual layer thickness of 50 nm were allowed to decay until the residual thickness increased to 266 nm [= ((360 × 240)/400 + 50) nm]. We calculated the diffraction efficiency for an incident angle of 64° and s-polarization (identical to the experimental condition, see Materials and Methods). The complex index of refraction of the silicon substrate at a wavelength of 405 nm was assumed to be 5.47 + 0.24*i*, while that of the PS was 1.49.

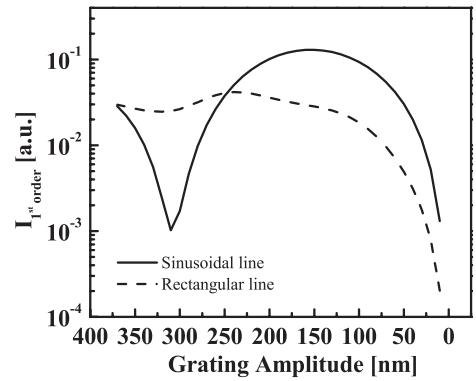

Figure 2. Diffraction efficiency of a grating with decreasing amplitude using the rigorous coupled wave approximation calculations (see the text for details). Two types of gratings were calculated; dashed and solid lines represent rectangular and sinusoidal line shape grating, respectively.

Figure 2 shows the results of the RCWA calculations. Clearly there are significant differences between the sinusoidal and rectangular profiles. However, in both cases, the decay of the first-order diffraction peak intensity is not monotonic and exhibits oscillations corresponding to resonance and interference in the structure. The diffraction intensity as a function of grating amplitude for the rectangular profile is reminiscent of the experimental data in Figure 1. The discrepancy between experiments and the RCWA calculations might come from the fact that changes in the line width during the annealing were not included in the RCWA calculations; small changes in the pattern width are expected in the actual pattern decay. Moreover, the line shape also evolves during the annealing and deviates from either a typical rectangular or sinusoidal cross section. Nevertheless, it appears that the non-monotonic variation in diffraction intensity can reasonably be attributed to optical resonance.

Figure 3 shows the first-order diffraction intensity measured as a function of annealing time for a PS1800k pattern at the bulk T_g (104 °C) of the polymer. The general trend is a decrease in the diffracted intensity as the pattern decays into the residual layer with time. Similar to the temperature dependence of the diffraction intensity (Figure 1), an intensity anomaly (local maximum) is also observed in the early stage of the annealing, due to the resonance effect.

In general, the scattering power (diffraction intensity) is proportional to the square of the scattering (diffraction) volume.[42] Since the pattern width does not vary much, the volume change of the grating lines is determined by their average height change.[36] Figure 3

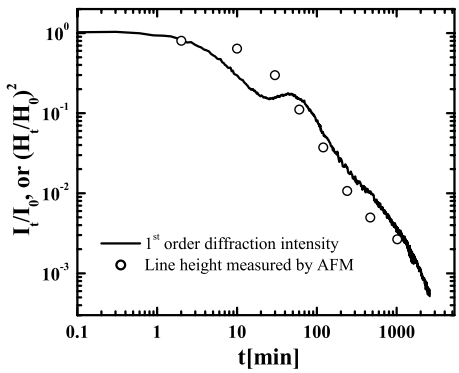

Figure 3. Comparison between the normalized diffraction intensity (I_t/I_0, solid lines) and the square of the normalized pattern height ($(H_t/H_0)^2$, open circles) as a function of annealing time at 104 °C. I_0 and H_0 represent the initial values of diffraction intensity from laser diffraction and pattern height from AFM measurements, respectively.

presents the pattern height (measured by atomic force microscopy, AFM) as a function of annealing time for the same sample under identical annealing conditions. To test the general relationship between diffraction intensity and sample volume, the square of the normalized pattern height (normalized by initial value, $(H_t/H_0)^2$, as a representative of the volume) is plotted as a function of annealing time in Figure 3. The volume/mass of the patterned PS measured by AFM decays monotonically, in contrast to the decay of diffraction intensity.

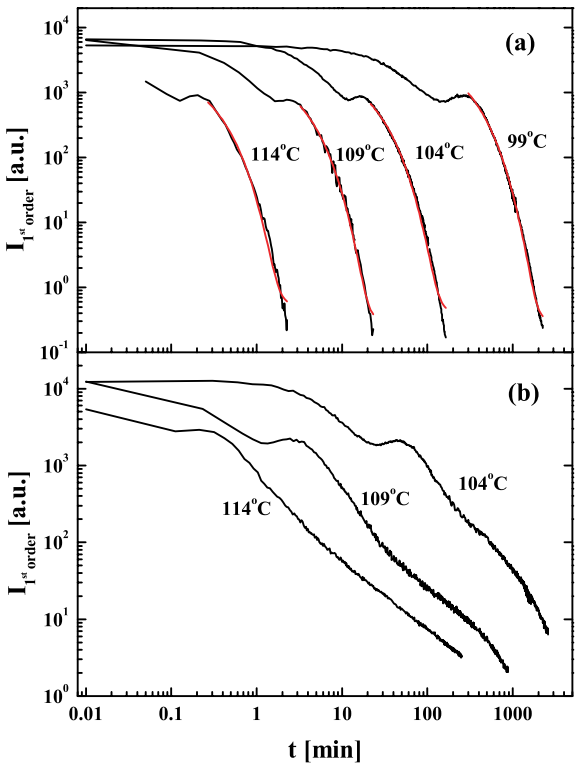

Figure 4. First-order intensity as a function of annealing time at different annealing temperatures for PS30k (a) and PS1800k (b). The annealing temperature decreases from the left to the right as 114, 109, 104, and 99 °C (for PS30k only). The red solid lines in panel a are the exponential fits of the diffraction intensity.

Clearly, the relationship between the diffraction intensity and the pattern volume becomes invalid in the presence of resonance effects during the early stage of annealing (Figure 3). However, when the pattern height becomes much smaller than the wavelength of the light, the simple scalar theory is expected to be applicable.[38,42] This relationship is clearly seen at the later stage of annealing in Figure 3, where the agreement between the pattern height and diffraction intensity is reasonably good. Consistent with this, Durig *et al*. used a similar light diffraction technique to study the decay of 70 nm tall PMMA gratings, and no clear resonance intensity variation was observed.[45]

Overall, the discrepancies between pattern height change (volume change) and diffraction intensity change can be understood in terms of optical resonance (early stage), pattern shape uncertainty (*i.e.*, the height change does not fully represent the volume change), and an increase of the Debye–Waller factor. The latter is caused by the increase in nonuniformity between different lines during the decay, causing an increase in diffuse scattering that will decrease the diffraction intensity. Diffuse scattering is negligible in patterns at early stages of annealing and accounts for less than 1% of the total incident radiation.[42] Nevertheless, the monotonic intensity decay of the late stage of the annealing is largely caused by pattern volume changes, represented by the pattern height.

3. Using the Resonance Diffraction To Characterize the Relaxation of Imprinted Patterns. Figure 4 shows the first-order diffraction intensity with annealing time at different temperatures for both the low- and high-molecular-mass PS patterns. The intensity decay reveals both similarity and discrepancy between the two samples. Both samples show the resonance anomaly discussed above at all temperatures. The corresponding time scale shifts to shorter time when the annealing is performed at higher temperatures. This time–temperature equivalence of the optical anomaly is consistent with the notion that it corresponds to a characteristic pattern shape/height (see Figure 3). From Figure 3, we can see that the maximum of the optical intensity anomaly roughly corresponds to the point when the pattern height decays to about 30% of its original height. In this respect, we can use the intensity anomaly as a marker, characteristic of a well-defined pattern shape/height, to compare the decay kinetics of the low- and high-molecular-mass patterns. On the other hand, pattern decay characteristics can also be compared on the basis of the intensity decay during the late stage of the pattern evolution, where the resonance anomaly does not interfere. Specifically, for PS30k, the decay kinetics at long times is well approximated by a single-exponential decay function (see the fit in Figure 4a). The exponential time constant is another characteristic parameter that may be used to compare the decay re-

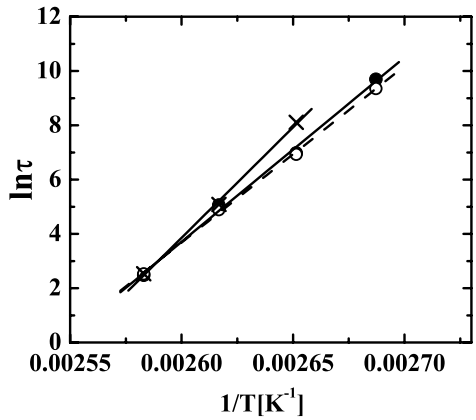

Figure 5. Arrhenius plots of the temperature dependence of the characteristic time (τ_m) when the maximum intensity of the anomaly occurs for PS30k (×) and PS1800k (●). The solid lines represent their linear fit. Open circles represent the exponential decay time from the fit for PS30k in Figure 4a, and the dashed line is its linear fit.

sponse at different temperatures. However, for PS1800k pattern, the intensity decay does not follow an exponential decay function. We will return to this observation shortly.

For each sample, the overall decay rate becomes faster with increasing temperature, indicating an increased molecular mobility, while the shape of the decay curve remains similar for each molecular mass of the PS (Figure 4). The apparent time–temperature superposition behavior is typical for the viscoelastic response of polymers.[46] In the bulk polymer, the temperature shift of the characteristic relaxation time (or viscosity) generally follows the classic Williams–Ferry–Landel equation for temperatures above T_g.[46] Here, we use the time at which the maximum of the intensity anomaly occurs (τ_m) during annealing at the different temperatures for both PS samples as the characteristic time constant (Figure 4). Figure 5 shows an Arrhenius plot for the temperature dependence of τ_m. Within the relatively narrow temperature range of the measurements (20 °C), the activation energy associated with this process is estimated to be 564 and 677 kJ/mol for PS30k and PS1800k, respectively. Figure 5 also displays the decay time constants from the exponential fit for the long-time decay kinetics of the PS30k sample in Figure 4a. Surprisingly, the exponential time constants are almost identical to the τ_m values extracted from the intensity anomaly in PS30k. The origin of this coincidence is not clear at this point.

Polymer relaxations occur over a range of lengths scales, relevant to the present discussion, from the segmental relaxations involving several monomer units to the whole chain relaxations associated with viscous flow. To understand the relaxation process associated with the pattern decay process, Figure 6 compares the temperature dependence of the intensity anomaly of the pattern decay (τ_m), the segmental relaxation of the glass transition (τ_α, measured by dielectric spectroscopy),[47] and the terminal time (τ_1, estimated from viscoelastic measurements as $\tau_1 \approx \eta_0 J_e^0$).[48] It is generally understood that τ_α has similar temperature dependence for the PS30k and PS1800k samples.[47] However, τ_1 depends strongly on the molecular mass of the chain, a characteristic property of polymers. Although it is known that τ_α has a stronger temperature dependence than τ_1 for most polymers,[49,50] it is usually assumed that the temperature dependence of τ_1, and all other relaxation modes, is determined by that of τ_α.[46] From Figure 6, it can be seen that the temperature dependence of τ_m is similar to that of τ_1 for PS30k, while it is closer to τ_α for PS1800k.

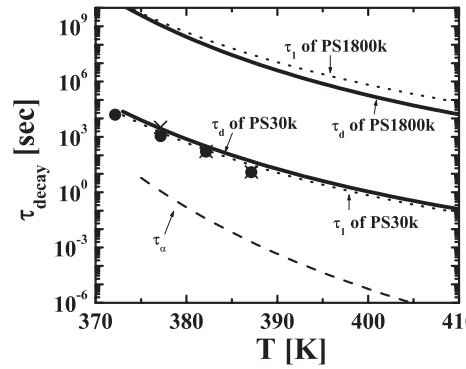

Figure 6. Temperature dependence of τ_m for PS30k (×) and PS1800k (●), same as in Figure 5. The dashed line shows the temperature dependence of the segmental relaxation time (τ_α) for a typical high-molecular-mass PS measured by dielectric spectroscopy.[47] The two solid lines represent the temperature dependence of the decay time (τ_d) of PS30k and PS1800k estimated from eq 2, with zero shear viscosity assumed. The dotted lines describe the terminal time (τ_1) for both PS30k and PS1800k from rheology measurements.[48] See the text for details.

The most surprising observation, however, is that there is no significant difference in τ_m between PS1800k and PS30k. Specifically, it takes about the same time for the patterns of PS1800k and PS30k to reach the same height/shape at which the resonance anomaly occurs, despite the huge difference in viscosity. Similar observations have been made in our previous study of pattern evolution using X-ray diffraction techniques for patterns with a much smaller feature size.[36] In that case, the initial decay rate of highly entangled PS patterns was *faster* than that of the unentangled ones. This phenomenon was caused by the difference in the driving force for the pattern decay between PS30k and PS1800k, as discussed in the following.

Multiple mechanisms can contribute to the pattern relaxation processes.[51] For a simple liquid, the relaxation rate depends on the balance between thermodynamic and kinetic parameters. The governing thermodynamic parameter is the surface tension ($\gamma \cong 0.033$ N/m) of PS, which induces a large Laplace pressure ($P = \gamma/R$) at the highly curved region, driving the initial pattern to level. The influence of the feature size (Γ) is reflected through the radius of the curvature R. The

resistance to driving force is determined by the effective viscosity (η) of the material, a kinetic parameter that depends strongly on the temperature and molecular mass of the polymer. For such a surface-tension-driven viscous flow, the amplitude (H) of a grating decays exponentially with time.[38] For a sinusoidal grating,

$$dH/dt = (-\pi\gamma H)/2\Gamma\eta \quad (1)$$

and the leveling decay time (τ_d) is

$$\tau_d = \eta\Gamma/\pi\gamma \quad (2)$$

Since the difference in γ between the PS30k and PS1800k samples is negligible for the given annealing temperatures and the initial patterns are identical, the decay of pattern height should be dominated by η. In the limit of linear rheology, the zero shear viscosity (η_0) strongly depends on the molecular mass of the polymer. For unentangled polymers, *i.e.*, $M < M_c$ (the critical molecular mass of entanglement), $\eta_0 \propto M^1$. For polymers with $M \gg M_c$, $\eta_0 \propto M^{3.4}$.[46] For PS, M_c is about 38 000, so it may be said that PS1800k is highly entangled and PS30k is marginally entangled or unentangled.[46] Therefore, η_0 of PS1800k is roughly 10^6 times greater than that of PS30k at the same temperature, implying that the decay time of PS1800k would be a million times longer in the steady-state limit. Figure 6 shows the τ_d estimated from eq 2 for the patterns of both PS samples with the temperature dependence of the η_0 obtained from ref 48. For PS30k, the rates of pattern decay characterized by both the exponential time τ_d and τ_m are both similar to the prediction from eq 2. Clearly, the mechanism for PS30k pattern decay is mainly surface-tension-driven viscous flow, with an apparent viscosity similar to η_0. This mechanism is consistent with the observation that diffraction intensity/pattern height in Figure 4a decays exponentially, as predicted from eq 1. On the other hand, the decay rate for PS1800k pattern is evidently much faster than that expected from such a simple scenario (Figure 6). In our case, this nonexponential fast initial decay of PS1800k is due to the residual stress induced during the NIL processing.[36]

NIL is a complicated rheological process and involves both shear and extensional flow of the polymers.[52–57] The type of flow involved is determined by the geometry of the mold (*e.g.*, the line/space ratio, the shape of the lines, *etc.*) and the initial film thickness.[54,56] In our case, shear flow dominates the mold filling, and the shear rate ($\dot{\gamma}$) varies during the imprinting process. The apparent shear rate from this geometry can be roughly estimated as[54]

$$\dot{\gamma} = 3sv/h^2 \quad (3)$$

where s is the width of the extruded part of the mold, h is the film thickness, and v is the advancing velocity of the mold, determined by the imprinting conditions (P, T) and material response. Using a real-time light diffraction technique, v has been measured to be about 20 nm/s for initial deformation.[58] Using this value, we thus estimate $\dot{\gamma}$ to be about 0.16 s^{-1} in our experiments. The viscoelastic response of PS under such a shear rate is determined by the temperature of the imprinting, which changes the reorientation time of the polymer chains at different length scales to relax the disrupted chain dimensions and stresses.

For PS30k at 20 °C above T_g, the terminal time (τ_1) for an entire chain relaxation is about 1.5 s (Figure 6). The maximum dimensionless flow rate $\dot{\gamma}\tau_1$ with respect to the chain-orientation relaxation rate is only 0.24, suggesting that the PS30k sample will have a Newtonian-like response during the imprint-induced flow. Moreover, even if any nonlinear viscoelastic deformation occurs during the flow, the duration of the imprinting (3 min; see Materials and Methods) is much larger than the reorientation time of the PS30k chain (τ_1). Therefore, any process-induced chain anisotropy will be mostly relaxed, and the chains should be, to a first approximation, in their unperturbed state. When such a pattern is heated above T_g, the only driving force is surface tension, and viscosity governs the deformation. The slightly smaller decay time observed in experiments compared with τ_d estimated from eq 2 (see Figure 6) might be caused by the large Laplace pressure associated with the sharp corners that might reduce the effective viscosity relative to η_0.

The evolution of the pattern decay is strikingly different in the entangled polymer films (PS1800k), where the imprinting temperature is also at 20 °C above T_g. Under this condition, τ_1 is on the order of 10^6 s (Figure 6). Correspondingly, the dimensionless flow rate $\dot{\gamma}\tau_1$ for PS1800k is on the order of 10^5, suggesting that, in this case, the imprinting process is in the strongly nonlinear viscoelastic deformation regime. Moreover, the duration of the NIL is about 200 s, which is clearly not enough for effective structural relaxation to occur. The internal stresses within this imprinted material then become "locked in" as the material is quenched below T_g. The residual stresses will contribute to the evolution of the surface patterns if the samples are heated back to a temperature at or above T_g. Therefore, the driving force for the decay of PS1800k patterns involves both the residual stresses and the thermodynamic driving forces, and the former effect can be expected to be predominant. This hypothesis is supported by the fact that the initial pattern decay for the entangled polymers can occur at a rate close to or even faster than the unentangled polymer melt.[36]

We can understand the qualitative origin of the viscoelastic response of these films by considering the rubbery consistency of this high-molecular-mass polymer melt under the imprinting conditions. According to the localization model of Gaylord and Douglas,[59,60] the tran-

sient elasticity of an "entangled" polymer melt in response to a deformation of the material as a whole derives from a distortion of the local tube-like environment about the chains in the melt. The number of conformations accessible to the chains is greatly reduced compared with that of isolated chains over the time scales that these tube-like regions persist ($t_p \approx \tau_1$), giving rise to a melt elasticity that is quite distinct from that arising from deforming a network of Gaussian chains fixed at their end points. An interesting aspect of this type of entropic elasticity is that this localization effect greatly diminishes upon stretching the material uniaxially (strain softening) or isotropic swelling.[61] In the present context, the above physical picture of chain "entanglement" implies that, if the distortion of the polymer melt occurs at a rate less than $1/\tau_1$, the relaxation of these distortions in the local polymer conformations should occur on a time scale associated with segmental motions rather than that of the chain as a whole. In other words, the deformation/flow process is dominated by the local chain modes, *i.e.*, Rouse-type modes (motion of part of the chains). Naturally, the relaxation of the local residual stresses associated with these local distortions occurs on a much shorter time scale than large-scale structural relaxation of the melt (τ_1). Similar effects of residual stress in highly entangled polymers, although having a different origin, have also been shown to play an important role in the dewetting dynamics of thin polymer films. In the dewetting studies, the hole-growth rate is found to be faster for higher molecular mass PS, consistent with residual stress effects playing a key role in the instability of these thin films.[62]

CONCLUSIONS

We have studied the evolution of polystyrene grating patterns made by nanoimprint lithography using *in situ* light diffraction during thermal annealing. A distinctive anomaly in diffraction intensity is observed during the annealing of these gratings with tall lines. The origin of this anomaly can be qualitatively understood as a resonance effect due to the interaction of the light with certain shapes/heights of the grating lines. It can serve as a characteristic time scale to analyze the pattern decay. The decay rate shifts to shorter time with increasing annealing temperature, and the temperature dependence this decay rate is similar to that of the segmental or chain relaxation.

Although the imprinting process causes no appreciable change of T_g for both the unentangled (PS30k) and highly entangled (PS1800k) imprinted patterns, it does significantly influence the stability of the patterns. For PS30k the pattern decay occurs as expected for a simple Newtonian fluid, while for PS1800k the relaxation of residual stresses significantly enhances the pattern decay process. The characteristic time scale of the abnormal resonance feature in the diffraction intensity provides a useful measure of the decay of the surface patterns, regardless of whether the pattern decay is driven by the surface energy or the residual stress derived from the imprinting process.

MATERIALS AND METHODS

Monodisperse PS samples with two different molar masses (M_n = 30 and 1800 kg/mol) were purchased from Polymer Laboratories and Pressure Chemical Co., respectively. The bulk T_g for both samples was measured by DSC with a heating/cooling rate of 10 °C/min. The values for both PS samples are about 104 °C.

Films of PS were prepared on silicon substrates by spin-casting from toluene solutions. The Si wafers had a thin native oxide surface that was cleaned in a UV–ozone cleaner (Jelight, model no. 42) for 1 min to remove organic residues. The concentration of the PS in the toluene was 5.5% by mass for PS30k and 2.8% by mass for PS1800k, and these solutions were spun at 209 rad/s (2000 rpm) for 1 min. The as-cast films were annealed in a vacuum oven at 170 °C for 1 h to remove the residual solvent. The thickness, as measured by SXR, was approximately 270 nm for both the PS30k and PS1800k films.

The imprint mold consisted of parallel line-and-space gratings in silicon oxide with periodicity Γ of 400 nm. To facilitate the mold separation process, a self-assembled monolayer of $CF_3(CF_2)_5(CH_2)_2SiCl_3$ (tridecafluoro-1,1,2,2-tetrahydrooctyltrichlorosilane) was developed onto the mold through a vapor-phase process.[63] The imprinting processes were performed on a Nanonex NX-2000 tool by heating the films to 20 °C above the T_g of the PS and applying a pressure of 3.4 MPa for 3 min. The sample was cooled to 55 °C before the pressure was released and the mold separated from the patterned PS films. An excellent fidelity of the pattern-transfer process was confirmed with SXR and AFM. The PS lines in the grating had pattern height $h \approx 360$ nm, width $w \approx 240$ nm, and residual layer thickness $d_{RL} \approx 50$ nm. A more detailed explanation of the pattern shape characterization using SXR can be found in refs 33 and 34.

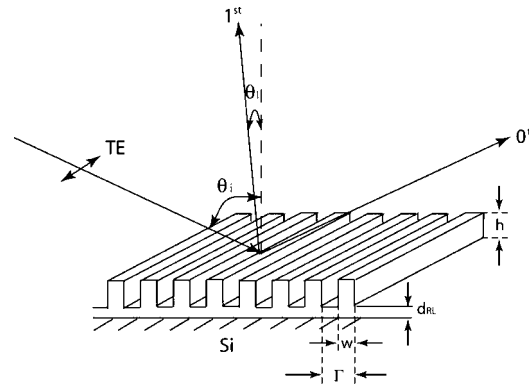

Figure 7. Geometry of the light diffraction experiments. The dimensions of an as-imprinted grating are shown. The incident angle θ_i and first-order diffraction angle θ_1 are shown relative to the grating normal. The polarization mode of the laser is transverse electric (TE). The pattern was placed horizontally on top of a heating stage in the thermal annealing experiments.

Figure 7 describes the laser diffraction experiments. The samples, with a patterned area of 5 mm × 5 mm, were mounted horizontally on a hot stage (Linkam, model THMS600) with precise temperature control (Linkam, model TMS94). A laser (λ = 405 nm) was directed at the film with the polarization of the beam parallel to the grating lines and perpendicular to the incident plane (transverse electric mode, or s-polarization). The inci-

dent angle of the beam relative to the normal of the grating surface, θ_i, was 64° ± 0.5° (the error bars presented throughout this manuscript indicate the relative standard uncertainty of the measurement). The grating equation,

$$\sin \theta_m = m\lambda/\Gamma - \sin \theta_i \quad (4)$$

determines the direction of the diffracted beam, where θ_m is the *m*th order of the diffraction peaks. In this case, for the first-order diffraction peak, $\theta_1 = 6.3°$, and all the other higher orders are evanescent. The first-order diffraction intensity as a function of annealing time or temperature was recorded with a CCD camera.

Certain commercial materials and equipment are identified in this paper in order to specify adequately the experimental procedure. In no case does such identification imply recommendation by the National Institute of Standards and Technology nor does it imply that the material or equipment identified is necessarily the best available for this purpose.

Acknowledgment. This work is partially funded by the NIST Office of Microelectronic Programs. B.C.O. recognizes the support of the National Research Council NIST Postdoc Fellowship Program. We thank Christopher Stafford, Kirt Page, and Thomas Chastek for their help with the experimental setup. We acknowledge the Nanofabrication Laboratory of the Center for Nanoscale Science and Technology (CNST) in NIST for providing facilities for the nanoimprinting process.

REFERENCES AND NOTES

1. Resnick, D. J.; Dauksher, W. J.; Mancini, D.; Nordquist, K. J.; Bailey, T. C.; Johnson, S.; Stacey, N.; Ekerdt, J. G.; Willson, C. G.; Sreenivasan, S. V.; Schumaker, N. Imprint Lithography for Integrated Circuit Fabrication. *J. Vac. Sci. Technol. B* **2003**, *21*, 2624–2631.
2. Bailey, T. C.; Johnson, S. C.; Sreenivasan, S. V.; Ekerdt, J. G.; Willson, C. G.; Resnick, D. J. Step and Flash Imprint Lithography: An Efficient Nanoscale Printing Technology. *J. Photopolym. Sci. Technol.* **2002**, *15*, 481–486.
3. Bailey, T. C.; Choi, B. J.; Colburn, M.; Meissl, M.; Shaya, S.; Ekerdt, J. G.; Sreenivasan, S. V.; Willson, C. G. Step and Flash Imprint Lithography: Template Surface Treatment and Defect Analysis. *J. Vac. Sci. Technol. B* **2000**, *18*, 3572–3577.
4. Jung, G. Y.; Johnston-Halperin, E.; Wu, W.; Yu, Z. N.; Wang, S. Y.; Tong, W. M.; Li, Z. Y.; Green, J. E.; Sheriff, B. A.; Boukai, A.; Bunimovich, Y.; Heath, J. R.; Williams, R. S. Circuit Fabrication at 17 nm Half-Pitch by Nanoimprint Lithography. *Nano Lett.* **2006**, *6*, 351–354.
5. Jung, G. Y.; Ganapathiappan, S.; Ohlberg, D. A. A.; Olynick, D. L.; Chen, Y.; Tong, W. M.; Williams, R. S. Fabrication of a 34 × 34 Crossbar Structure at 50 nm Half-Pitch by UV-based Nanoimprint Lithography. *Nano Lett.* **2004**, *4*, 1225–1229.
6. Cheng, X.; Guo, L. J.; Fu, P. F. Room-Temperature, Low-pressure Nanoimprinting Based on Cationic Photopolymerization of Novel Epoxysilicone Monomers. *Adv. Mater.* **2005**, *17*, 1419–1424.
7. Stewart, M. D.; Johnson, S. C.; Sreenivasan, S. V.; Resnick, D. J.; Willson, C. G. Nanofabrication with Step and Flash Imprint Lithography. *J. Microlith., Microfab., Microsyst.* **2005**, *4*011002.
8. Chou, S. Y.; Krauss, P. R.; Renstrom, P. J. Imprint Lithography with 25-Nanometer Resolution. *Science* **1996**, *272*, 85–87.
9. Chou, S. Y.; Krauss, P. R.; Renstrom, P. J. Imprint of Sub-25 nm VIAS and Trenches in Polymers. *Appl. Phys. Lett.* **1995**, *67*, 3114–3116.
10. Chou, S. Y.; Krauss, P. R.; Renstrom, P. J. Nanoimprint Lithography. *J. Vac. Sci. Technol. B* **1996**, *14*, 4129–4133.
11. Austin, M. D.; Ge, H. X.; Wu, W.; Li, M. T.; Yu, Z. N.; Wasserman, D.; Lyon, S. A.; Chou, S. Y. Fabrication of 5 nm Linewidth and 14 nm Pitch Features by Nanoimprint Lithography. *Appl. Phys. Lett.* **2004**, *84*, 5299–5301.
12. Guo, L. J. Recent Progress in Nanoimprint Technology and its Applications. *J. Phys. D: Appl. Phys.* **2004**, *37*, R123–R141.
13. Chou, S. Y.; Krauss, P. R. Imprint Lithography with Sub-10 nm Feature Size and High Throughput. *Microelect. Eng.* **1997**, *35*, 237–240.
14. Cross, G. L. W. The Production of Nanostructures by Mechanical Forming. *J. Phys. D: Appl. Phys.* **2006**, *39*, R363–R386.
15. Scheer, H. C.; Schulz, H.; Hoffmann, T.; Torres, C. M. S. Problems of the Nanoimprinting Technique for Nanometer Scale Pattern Definition. *J. Vac. Sci. Technol. B* **1998**, *16*, 3917–3921.
16. Cross, G. L. W.; O'Connell, B. S.; Ozer, H. O.; Pethica, J. B. Room Temperature Mechanical Thinning and Imprinting of Solid Films. *Nano Lett.* **2007**, *7*, 357–362.
17. Scheer, H. C.; Schulz, H. A Contribution to the Flow Behavior of Thin Polymer Films during Hot Embossing Lithography. *Microelect. Eng.* **2001**, *56*, 311–332.
18. Behl, M.; Seekamp, J.; Zankovych, S.; Torres, C. M. S.; Zentel, R.; Ahopelto, J. Towards Plastic Electronics: Patterning Semiconducting Polymers by Nanoimprint Lithography. *Adv. Mater.* **2002**, *14*, 588–591.
19. Mele, E.; Di Benedetto, F.; Persano, L.; Cingolani, R.; Pisignano, D. Multilevel, Room-Temperature Nanoimprint Lithography for Conjugated Polymer-Based Photonics. *Nano Lett.* **2005**, *5*, 1915–1919.
20. Ro, H. W.; Jones, R. L.; Peng, H.; Hines, D. R.; Lee, H. J., Lin, E. K.; Karim, A.; Yoon, D. Y.; Gidley, D. W.; Soles, C. L. The Direct Patterning of Nanoporous Interlayer Dielectric Insulator Films by Nanoimprint Lithography. *Adv. Mater*. In press.
21. Arakcheeva, E. M.; Tanklevskaya, E. M.; Nesterov, S. I.; Maksimov, M. V.; Gurevich, S. A.; Seekamp, J.; Torres, C. M. S. Fabrication of Semiconductor- and Polymer-Based Photonic Crystals Using Nanoimprint Lithography. *Tech. Phys.* **2005**, *50*, 1043–1047.
22. Li, H. W.; Huck, W. T. S. Ordered Block-Copolymer Assembly Using Nanoimprint Lithography. *Nano Lett.* **2004**, *4*, 1633–1636.
23. Hu, Z. J.; Baralia, G.; Bayot, V.; Gohy, J. F.; Jonas, A. M. Nanoscale Control of Polymer Crystallization by Nanoimprint Lithography. *Nano Lett.* **2005**, *5*, 1738–1743.
24. Okerberg, B. C.; Soles, C. L.; Douglas, J. F.; Ro, H. W.; Karim, A.; Hines, D. R. Crystallization of Poly(ethylene oxide) Patterned by Nanoimprint Lithography. *Macromolecules* **2007**, *40*, 2968–2970.
25. Alcoutlabi, M.; McKenna, G. B. Effects of Confinement on Material Behavior at the Nanometer Size Scale. *J. Phys. Condens. Matter* **2005**, *17*, R461–R524, and references cited therein.
26. Stafford, C. M.; Vogt, B. D.; Harrison, C.; Julthongpiput, D.; Huang, R. Elastic Moduli of Ultrathin Amorphous Polymer Films. *Macromolecules* **2006**, *39*, 5095–5099.
27. Van Workum, K.; de Pablo, J. J. Computer Simulation of the Mechanical Properties of Amorphous Polymer Nanostructures. *Nano Lett.* **2003**, *3*, 1405–1410.
28. Soles, C. L.; Douglas, J. F.; Jones, R. L.; Wu, W. L. Unusual Expansion and Contraction in Ultrathin Glassy Polycarbonate Films. *Macromolecules* **2004**, *37*, 2901–2908.
29. Larson, R. G. *Constitutive Equations for Polymer Melts and Solutions*; Butterworths: Boston, 1988.
30. Jones, R. L.; Hu, T.; Lin, E. K.; Wu, W. L.; Kolb, R.; Casa, D. M.; Bolton, P. J.; Barclay, G. G. Small Angle X-Ray Scattering for Sub-100 nm Pattern Characterization. *Appl. Phys. Lett.* **2003**, *83*, 4059–4061.
31. Hu, T. J.; Jones, R. L.; Wu, W. L.; Lin, E. K.; Lin, Q. H.; Keane, D.; Weigand, S.; Quintana, J. Small Angle X-Ray Scattering Metrology for Sidewall Angle and Cross Section of Nanometer Scale Line Gratings. *J. Appl. Phys.* **2004**, *96*, 1983–1987.
32. Jones, R. L.; Hu, T. J.; Soles, C. L.; Lin, E. K.; Hu, W.; Reano, R. M.; Pang, S. W.; Casa, D. M. Pattern Fidelity in Nano-imprinted Films Using Critical Dimension Small Angle X-

Ray Scattering. *J. Microlith., Microfab., Microsyst.* **2005**, *5*013001.
33. Lee, H. J.; Soles, C. L.; Ro, H. W.; Jones, R. L.; Lin, E. K.; Wu, W. L.; Hines, D. R. Nanoimprint Pattern Transfer Quality from Specular X-Ray Reflectivity. *Appl. Phys. Lett.* **2005**, *87*263111.
34. Lee, H. J.; Ro, H. W.; Soles, C. L.; Jones, R. L.; Lin, E. K.; Wu, W. L.; Hines, D. R. Effect of Initial Resist Thickness on Residual Layer Thickness of Nanoimprinted Structures. *J. Vac. Sci. Technol. B* **2005**, *23*, 3023–3027.
35. Jones, R. L.; Hu, T. J.; Soles, C. L.; Lin, E. K.; Reano, R. M.; Casa, D. M. Real-Time Shape Evolution of Nanoimprinted Polymer Structures During Thermal Annealing. *Nano Lett.* **2006**, *6*, 1723–1728.
36. Ding, Y.; Ro, H. W.; Douglas, J. F.; Jones, R. L.; Hines, D. R.; Karim, A.; Soles, C. L. Polymer Viscoelasticity and Residual Stress Effects on Nanoimprint Lithography. *Adv. Mater.* **2007**, *19*, 1377–1382.
37. Peterson, K.; Johannsmann, D. Measurements on the Surface Glass Transition of PMMA from the Decay of Imprinted Surface Corrugation Gratings: the Influence of Molecular Weight. *J. Non-Cryst. Solids* **2002**, *307–310*, 532–537.
38. Hamdorf, M.; Johannsmann, D. Surface-Rheological Measurements on Glass Forming Polymers Based on the Surface Tension Driven Decay of Imprinted Corrugation Gratings. *J. Chem. Phys.* **2000**, *112*, 4262–4270.
39. Mundra, M. K.; Donthu, S. K.; Dravid, V. P.; Torkelson, J. M. Effect of Spatial Confinement on the Glass-Transition Temperature of Patterned Polymer Nanostructures. *Nano Lett.* **2007**, *7*, 713–718.
40. Buck, E.; Petersen, K.; Hund, M.; Krausch, G.; Johannsmann, D. Decay Kinetics of Nanoscale Corrugation Gratings on Polymer Surface: Evidence for Polymer Flow Below the Glass Temperature. *Macromolecules* **2004**, *37*, 8647–8652.
41. Kerle, T.; Lin, Z. Q.; Kim, H. C.; Russell, T. P. Mobility of Polymers at the Air/Polymer Interface. *Macromolecules* **2001**, *34*, 3484–3492.
42. Loewen, E. G.; Popov, E. *Diffraction Gratings and Applications*; Marcel Dekker: New York, 1997.
43. Moharam, M. G.; Grann, E. B.; Pommet, D. A.; Gaylord, T. K. Formulation for Stable and Efficient Implementation of the Rigorous Couple-Wave Analysis of Binary Gratings. *J. Opt. Soc. Am. A* **1995**, *12*, 1068–1076.
44. Moharam, M. G.; Pommet, D. A.; Grann, E. B.; Gaylord, T. K. Stable Implementation of the Rigorous Coupled-Wave Analysis for Surface-Relief Gratings—Enhanced Transmittance Matrix Approach. *J. Opt. Soc. Am. A* **1995**, *12*, 1077–1086.
45. Durig, U.; Cross, G.; Despont, M.; Drechsler, U.; Haberle, W.; Lutwyche, M. I.; Rothuizen, H.; Stutz, R.; Widmer, R.; Vettiger, P.; Binnig, G. K.; King, W. P.; Goodson, K. E. "Millipede"—An AFM Data Storage System at the Frontier of Nanotribology. *Tribol. Lett.* **2000**, *9*, 25–32.
46. Ferry, J. D. *Viscoelastic Properties of Polymers*, 3rd ed.; John Wiley & Sons: New York, 1980.
47. Santangelo, P. G.; Roland, C. M. Molecular Weight Dependence of Fragility in Polystyrene. *Macromolecules* **1998**, *31*, 4581–4585.
48. Majeste, J. C.; Montfort, J. P.; Allal, A.; Marin, G. Viscoelasticity of Low Molecular Weight Polymers and the Transition to the Entangled Regime. *Rheol. Acta* **1998**, *37*, 486–499.
49. Ngai, K. L.; Plazek, D. J. Identification of Different Modes of Molecular-Motion in Polymers that Cause Thermorheological Complexity. *Rubber Chem. Technol., Rubber Rev.* **1995**, *68*, 376–434, and references cited therein.
50. Ding, Y. F.; Sokolov, A. P. Breakdown of Time-Temperature Superposition Principle and Universality of Chain Dynamics in Polymers. *Macromolecules* **2006**, *39*, 3322–3326.
51. Mullins, W.W. Theory of Thermal Grooving. *J. Appl. Phys.* **1959**, *30*, 77–83.
52. Hirai, Y.; Yoshida, S.; Takagi, N. Defect Analysis in Thermal Nanoimprint Lithography. *J. Vac. Sci. Technol. B* **2003**, *21*, 2765–2770.
53. Hirai, Y.; Yoshida, S.; Takagi, N.; Tanaka, Y.; Yabe, H.; Sasaki, K.; Sumitani, H.; Yamamoto, K. High Aspect Pattern Fabrication by Nanoimprint Lithography Using Fine Diamond Mold. *Jpn. J. Appl. Phys.* **2003**, *42*, 3863–3866.
54. Schulz, H.; Wissen, M.; Bogdanski, N.; Scheer, H. C.; Mattes, K.; Friedrich, C. Impact of Molecular Weight of Polymers and Shear Rate Effects for Nanoimprint Lithography. *Microelect. Eng.* **2006**, *83*, 259–280.
55. Schulz, H.; Wissen, M.; Bogdanski, N.; Scheer, H. C.; Mattes, K.; Friedrich, C. Choice of the Molecular Weight of An Imprint Polymer for Hot Embossing Lithography. *Microelect. Eng* **2005**, *78–79*, 625–632.
56. Rowland, H. D.; Sun, A. C.; Schunk, P. R.; King, W. P. Impact of Polymer Film Thickness and Cavity Size on Polymer Flow during Embossing: Toward Process Design Rules for Nanoimprint Lithography. *Micromech. Microeng.* **2005**, *15*, 2414–2425.
57. Scheer, H. C.; Bogdanski, N.; Wissen, M.; Konishi, T.; Hirai, Y. Polymer Time Constants During Low Temperature Nanoimprint Lithography. *J. Vac. Sci. Technol. B* **2005**, *23*, 2963–2966.
58. Yu, Z. N.; Gao, H.; Chou, S. Y. In situ Real Time Process Characterization in Nanoimprint Lithography Using Time-Resolved Diffractive Scatterometry. *Appl. Phys. Lett.* **2004**, *85*, 4166–4168.
59. Gaylord, R. J.; Douglas, J. F. Rubber Elasticity—A Scaling Approach. *Polym. Bull.* **1987**, *8*, 347–354.
60. Gaylord, R. J.; Douglas, J. F. The Localization Model of Rubber Elasticity—2. *Polym. Bull.* **1990**, *23*, 529–533.
61. Mark, J. E.; Erman, B. *Elastomeric Polymer Network*; Prentice-Hall: Englewood Cliffs, NJ, 1992;. Chapter 23.
62. Xavier, J. H.; Li, C.; Rafailovich, M. H.; Sokolov, J. Dynamics of Ultrathin Films in the Glassy State. *Langmuir* **2005**, *21*, 5069–5072.
63. Jung, G. Y.; Li, Z.; Wu, W.; Chen, Y.; Olynick, D. L.; Wang, S. Y.; Tong, W. M.; Williams, R. S. Vapor-Phase Self-assembled Monolayer for Improved Mold Release in Nanoimprint Lithography. *Langmuir* **2005**, *21*, 1158–1161.